

## Analysis of Neutrino Oscillation Data with the Recent KamLAND results

P. Aliani<sup>†1</sup>, V. Antonelli<sup>\*1</sup>, R. Ferrari<sup>\*1</sup>, M. Picariello<sup>\*1</sup>, E. Torrente-Lujan<sup>©1</sup>

<sup>†</sup> *Service de Physique Théorique, Univ. Libre de Bruxelles, Bruxelles, Belgium,*

<sup>\*</sup> *Dip. di Fisica, Univ. di Milano, and INFN Sez. Milano, Via Celoria 16, Milano, Italy*

<sup>©</sup> *Dept. de Fisica, Grupo de Fisica Teorica, Univ. de Murcia, Murcia, Spain*

### Abstract

We present an updated analysis of all available solar and reactor neutrino data, emphasizing in particular the totality of the KamLAND results including the *SNO* phase II (NaCl) spectrum data. In a two active-neutrino framework, we determine the solutions in the  $\Delta m_{\odot}^2, \tan^2 \theta_{\odot}$  parameter space compatible with experimental data using a  $\phi$ -distribution technique where the gaussian approximation is not acceptable. Combining all data, we obtain the following best-fit parameters:  $\Delta m_{\odot}^2 = 8.17 \times 10^{-5} \text{eV}^2$ ,  $\tan^2 \theta_{\odot} = 0.40$ . The impact of these results is discussed.

PACS: 26.65.+t, 14.60.Pq

## 1 Introduction

Evidence of antineutrino disappearance in a beam of antineutrinos in the Kamland experiment has been presented [1]. The analysis of the experimental results on reactor physics and solar neutrinos [2] in terms of neutrino oscillations has largely improved our knowledge of neutrino mixing.

The recent KamLAND results confirm the previous data and give a more stringent limit on the neutrino mass parameters.

The solar neutrino data prior to September 7, 2003 converged to two distinct regions in the parameter space, often referred to as LMAI (centered around the best-fit point of  $\Delta m_{\odot}^2 = 7.1 \times 10^{-5} \text{eV}^2$ ,  $\tan^2 \theta_{\odot} = 0.47$ ) and LMAII (centered around  $\Delta m_{\odot}^2 = 1.5 \times 10^{-4} \text{eV}^2$ ,  $\tan^2 \theta_{\odot} = 0.48$ ). The inclusion of the last year's SNO data eliminated the LMAII region at about  $4\sigma$ , and the new KamLAND information further excludes the LMAII region ( $\approx 5\sigma$ ). The recent KamLAND results modify the best-fit point position in the parameter space and the collaboration gives [1] a  $\Delta m_{\odot}^2 = 8.2 \times 10^{-5} \text{eV}^2$  and  $\tan^2 \theta = 0.40$ . The aim of this work is to present a comprehensive updated analysis of all recent solar neutrino data including the KamLAND reactor-experiment results to determine the extent of the remaining viable region in the parameter space.

The structure of this paper is the following: in section 2 discuss our approach to the latest KamLAND results. All solar neutrino experiments are discussed in section 3. We discuss the importance of the SNO data and the spectrum results in section 3.1. We then proceed, in section 4, to explain the procedure adopted in our analysis and in section 5 we present our results. Finally we summarize and conclude in section 6.

---

<sup>1</sup>e-mails: paola.aliანი@ulb.ac.be, vito.antonelli@mi.infn.it, ruggero.ferrari@mi.infn.it, marco.picariello@mi.infn.it, emilio.torrente-lujan@cern.ch

## 2 KamLAND

### 2.1 The experimental setup

Reactor anti-neutrinos with energies above 1.8 MeV produced in some 53 commercial reactors are detected in the KamLAND detector via the inverse  $\beta$ -decay reaction  $\bar{\nu}_e + p \rightarrow n + e^+$ . The mean reactor-detector distance and energy window of these  $\bar{\nu}_e$  makes KamLAND an ideal testing ground for the LMA region of the  $\nu_\odot$  parameter space. The first results published by the KamLAND collaboration eliminated all possible solutions to the solar neutrino problem (SNP) except the LMA region of the parameter space [3]. The sensitivity of this experiment to the  $\Delta m^2$  parameter divided the previously whole LMA region into two distinct regions, the one relative to the smaller mass-squared difference being preferred by data [4]. Recently, the KamLAND collaboration has announced the new results: they give the results of the data taken from October to Jan 2004, corresponding to about 317 days live time. The collaboration has taken all data and in the analysis, has included the previous set. The most significant changes in the analysis technique are related to the fiducial volume definition. Whereas in the previous work, events taking place at the outer edge of the nylon balloon were rejected, the recent analysis adopts a more sophisticated coincidence-measurement technique to exclude unwanted backgrounds. The estimated error on initial  $\phi_0(\bar{\nu}_e)$  is of 2%, and a discussions between scientists and representatives of the commercial reactors has allowed the KamLAND collaboration to estimate the incoming neutrino flux with better accuracy. A graph of the variation of initial flux throughout the period of data taking is shown in fig. 1.a of [1].

#### 2.1.1 Our simulations

In order to correctly model the detector and incorporate it into our solar neutrino analysis, we used a constant, time-averaged fuel composition for all of the commercial reactors within detectable distance of the Kamioka site, namely  $^{235}\text{U} = 56.3\%$ ,  $^{238}\text{U} = 7.9\%$ ,  $^{239}\text{Pu} = 30.1\%$ , and  $^{241}\text{Pu} = 5.7\%$ . We used the full cross-section including electron recoil corrections. We analyzed the data above threshold of 2.6 MeV, as the low-energy end of the spectrum had effectively no events. We exclude, for the same reasons, the last bin. We neglected all backgrounds in our analysis, including geological background above 2.6 MeV. We use the resolutions published by the collaboration for the two different data sets, namely  $\sigma(E) = 6.2\%/\sqrt{E}$  for the recent data and  $\sigma(E) = 7.3\%/\sqrt{E}$  for data previously published.

In order to use all the data available, we use our montecarlo to estimate an equivalent efficiency for the two pre-upgrade and post-upgrade phases. In this way, we can determine an effective efficiency which takes the upgrade into account. The information relative to the no-oscillation initial flux for the two periods can be extracted from fig. 1.a of [1]. In their report, the collaboration gives an energy resolution  $\sigma/E$  of about 6.2% at 1 MeV, and bins ranging from 1.8 MeV to 8.5 MeV, although the lower energy bins are more affected by geo-neutrino backgrounds and are excluded from the analysis. The total systematic error is estimated at 6.5%. The spectrum can be deduced from fig. 2.a of [1] and is summarized in table [4].

The collaboration adopts a hybrid statistical technique to account for the non-gaussian high energy bins, where the number of events are insufficient. The measure suited to samples from a multinomial distribution, the Pearson- $\chi^2$ , can be generalized to work with samples from arbitrary asymptotic multivariate distributions. This corresponds to the transition from independent an system to a correlated one. Because we want to take into account the correlation between the systematic errors, we do not use the Pearson- $\chi^2$ , but its generalization, the  $\phi$ -distribution in order to take systematic effects into account. Furthermore, we assume full correlation between the different bins.

No MSW effects are taken into consideration for the KamLAND data alone, as it was shown that any asymmetry due to matter effects is negligible for  $\Delta m^2$  of the order of  $10 \times 10^{-5} \text{ eV}^2$ .

### 3 Solar data

The most ponderous data present in our analysis come from the solar neutrino experiments. The experimental results are compared to an expected signal which we compute numerically by convoluting the solar neutrino fluxes [5], oscillation probability at the detector location and detector response functions. Details of the numerical techniques used in this analysis can be found elsewhere [6]. Double-binned day-night and zenith angle bins are computed in order to analyze the full SuperKamiokande data [7], whereas single-binned data is used for the SNO detector [8–10]. The global signals only are used for the radiochemical experiments Homestake [11], SAGE [12, 13], GallEx [14] and GNO [15]. In particular, we want to draw attention to the fact that we have used both the global *and* the spectrum data of the phase-II SNO results.

#### 3.1 The Sudbury Neutrino Observatory

The Sudbury Neutrino Observatory (SNO) collaboration has presented data relative to the NaCl phase of the experiment [8]. The addition of NaCl to a pure D<sub>2</sub>O detection medium has the effect of increasing the detector’s sensitivity to the neutral-current (NC) reactions within its fiducial volume. The NC detection efficiency has changed from a previous ‘no-salt’ phase of approximately a factor three (the efficiency being a position-related quantity, we see that the increase is even bigger for distant events (see fig. 1a of [8])). This novelty has made it possible for the SNO collaboration to analyze their data without making use of the no-spectrum-distortion hypothesis. Furthermore, they have adopted a new ‘event topology’ criterion to distinguish among the different channels within the detector.

The SNO detector was planned to run on a three-phase program (for a comprehensive coverage of the SNO potentiality, see [16]). Being a heavy-water Cherenkov detector, it is sensitive to three neutrino interactions: elastic scattering (ES)  $\nu_w + e^- \rightarrow \nu_x + e^-$ , charged-current (CC)  $\nu_e + d \rightarrow e^- + 2p$  and neutral current (NC)  $\nu_x + d \rightarrow p + n + \nu_x$ . During the first phase of operation, data relative only to the first two of these was collected [9]. Successively, the NC reaction was tagged [10]. This reaction, which is equally sensitive to all neutrino flavors, is a fundamental experimental result, as it not only gives a direct measurement of the <sup>8</sup>B flux, but also represents a direct measurement of non-electron-flavor neutrinos originating in the sun. Unfortunately, although the second-phase results proved essential in confirming the oscillation hypothesis, the efficiency with which the NC reactions were detected at SNO was quite low. The results depended heavily on the explicit assumption that the neutrino spectrum be non-distorted, an assumption that is fortunately true in the LMA region of the parameter space although misleading in the MSW regime. It was perhaps this observation that pushed certain authors to analyze the effects of varying the weight of the matter interaction term in the neutrino propagation Hamiltonian [17]. In this context, it was shown that despite the extraordinary amount of solar neutrino data in our possession, if a fit to different ‘weights’ of the matter interaction term did not prefer in a significant way the classical MSW solution, and in fact, the data did not exclude the no-MSW effect hypothesis [17]. This analysis has been carried out again with the new SNO data. The inclusion of this data seems to exclude the null hypothesis at  $5.6\sigma$  [18].

The addition of NaCl to the pure heavy water in the SNO detector has the effect of drastically increasing the detector’s sensitivity to the NC reaction. The <sup>35</sup>Cl acting as receptors for the neutrons emitted in the NC reaction, produce a cascade of photons which are easier to detect. The NC signal was tagged as being a ‘multiple- $\gamma$ ’ event as opposed to the ‘single- $\gamma$ ’ CC and ES signals in this new data set.

The SNO Collaboration has now devised a new data-analysis technique which relies on the topology of the three different events. The new parameter ( $\beta_\ell$ ) relative to which they marginalize is known as the ‘isotropy’ of the Cherenkov light distribution was used to separate the CC, ES and NC signals, something

that was not possible in the previous two data sets. The measured fluxes as reported in [8] are:

$$\begin{aligned}\phi_{CC}^{\text{SNO}} &= 1.59_{-0.07}^{+0.08} \text{ (stat)} \quad {}_{-0.08}^{+0.06} \text{ (syst)} \\ \phi_{\text{ES}}^{\text{SNO}} &= 2.21_{-0.26}^{+0.31} \text{ (stat)} \pm 0.10 \text{ (syst)} \\ \phi_{\text{NC}}^{\text{SNO}} &= 5.21 \pm 0.27 \text{ (stat)} \pm 0.38 \text{ (syst)}\end{aligned}\tag{1}$$

(2)

yielding a CC/NC ratio of

$$\phi_{CC}^{\text{SNO}} / \phi_{\text{NC}}^{\text{SNO}} = 0.306 \pm 0.026 \text{ (stat)} \pm 0.38 \text{ (syst)}\tag{3}$$

For the purpose of their analyses, the SNO collaboration did not make use of the spectral information to produce their contour plots (see the SNO HOWTO for details [19]), both for simplicity and scarcity of information contained in the data itself. Nonetheless, we make use of all published data and refer the reader to section 4 for details.

The comparison of the new SNO results and the previous phase-II data can easily be made because the SNO collaboration has included in the recent paper results which were obtained following their previous method, along with the new unconstrained data. The new results are compatible with the previous ones. It seems that the overall effect of un-constraining the analysis is an increase in the measured fluxes, although the estimated total  $\Phi_B$  has decreased relative to the previous best-fit value, leaving even less space for eventual sterile neutrinos.

## 4 Our analysis

We use a standard  $\chi^2$  technique to test the non-oscillation hypothesis. Two different sets of analyses are possible with the present data on neutrino oscillations: 1) short-baseline reactor data, solar data including the SK spectrum and previous phase-I (CC only) SNO spectrum, phase-II SNO global result, combined with new the KamLAND spectrum and, 2) the previous set with the use of the phase-II SNO spectrum result and the new KamLAND data. In order to use all the SNO data, we consider the phase-I and phase-II results as two distinct but fully correlated experiments.

In all cases, the  $\chi^2$  for the global rates of the radiochemical experiments are

$$\chi_{\text{rad}}^2 = (\mathbf{R}^{\text{th}} - \mathbf{R}^{\text{exp}})^T (\sigma_{\text{corr}} + \sigma_{\text{uncor}})^{-1} (\mathbf{R}^{\text{th}} - \mathbf{R}^{\text{exp}}),\tag{4}$$

where  $\mathbf{R}^{\text{th,exp}}$  are length-two vectors containing the theoretical (or experimental) signal-to-no-oscillation expectation for the chlorine and gallium experiments. Correlated systematic and uncorrelated statistical errors are considered in  $\sigma_{\text{syst}}$  and  $\sigma_{\text{stat}}$  respectively. Note that the parameter-dependent  $R^{\text{th}}$  is an averaged day-night quantity, as the radiochemical experiments are not sensitive to day-night variations.

We consider the double-binned SK spectrum comprising of 8 energy bins for a total of 6 night bins and one day bin. The  $\chi^2$  is given by

$$\chi_{\text{SK}}^2 = (\alpha \mathbf{R}^{\text{th}} - \mathbf{R}^{\text{exp}})^T (\sigma_{\text{unc}}^2 + \sigma_{\text{cor}}^2)^{-1} (\alpha \mathbf{R}^{\text{th}} - \mathbf{R}^{\text{exp}}).\tag{5}$$

The covariance matrix  $\sigma$  is a 4-rank tensor containing information relative to the statistical errors and energy and zenith-angle bin-correlated and uncorrelated uncertainties. Since the publication of the first SNO NC results, we have adopted their estimate of  $\phi_B$  and incorporated the new parameter  $\alpha$  in the  $\chi^2$  representing the normalization with respect to this quantity. In determining our best-fit points, we minimize with respect to it.

As discussed in section 2.1.1, we use an alternative technique for the KamLAND data due to the low statistics of the high energy bins. Furthermore, in order to use all the available data, we determine overall

detector efficiencies for the pre- and post- PMT/electronics upgrade phases and use them subsequently in our analysis.

The total KamLAND contribution to the  $\chi^2$  is therefore:

$$\chi_{\text{KL}}^2 = \chi_{\text{KL, glob}}^2 + \chi_{\text{KL, } \phi}^2 \quad (6)$$

where

$$\chi_{\text{KL, glob}}^2 = \frac{(R^{\text{th}} - R^{\text{exp}})^2}{\sigma_{\text{stat+sys}}^2} \quad (7)$$

In the evaluation of  $\chi_{\text{KL, } \phi}^2$  we use vectors that comprise therefore of 13 spectral points of width 0.425 MeV. We have studied the influence of the systematic errors on the KamLAND response function and incorporated them in our correlation matrix. We assume full correlation among the different bins. Note that the quantities  $\mathbf{R}^{\text{exp}}$  and  $\mathbf{R}^{\text{th}}$  contain the number of events normalized to the no-oscillation scenario. Due to the fact that at high energy KamLAND observes a small number of events, we cannot use a Gaussian approximation for all bins. This means that the correlated systematic deviations cannot be introduced in a straightforward way. The  $\phi$ -distribution is used for those bins and refer the reader to the literature for discussions on the applicability of this method [20].

#### 4.1 Global SNO signal and other neutrino oscillation data

We recall that two analyzes of the SNO data are presented. The first considers the phase-II global signal alone, the second incorporates the phase-II spectrum.

For the purpose of this analysis, the  $\chi^2$  can be considered as the sum of three distinct contributions:

$$\chi^2 = \chi_{\text{KL}}^2 + \chi_{\odot/\text{SNO}}^2 + \chi_{\text{glob, SNO}}^2 \quad (8)$$

where  $\chi_{\text{KL}}^2$  is as in eq. 7.

We define  $\chi_{\odot/\text{SNO}}^2$  as the contribution of all solar neutrino experiments except SNO, i.e. (see eq. 4, 7):

$$\chi_{\odot/\text{SNO}}^2 = \chi_{\text{rad}}^2 + \chi_{\text{SK}}^2 \quad (9)$$

The SNO contribution is given by

$$\chi_{\text{glob, SNO}}^2 = (\mathbf{R}^{\text{th}} - \mathbf{R}^{\text{exp}})^T (\sigma_{\text{corr}} + \sigma_{\text{syst}})^{-1} (\mathbf{R}^{\text{th}} - \mathbf{R}^{\text{exp}}) \quad (10)$$

where  $\mathbf{R}^{\text{th, exp}}$  are length-14 vectors containing the phase-II spectrum data (13 bins) and the new phase-III global SNO result. We consider the two SNO results as if coming from two independent experiments, but fully correlated. We use the backgrounds as listed in table 1 of [10] for the phase-II data, and the detector resolution given in the HOWTO.

#### 4.2 The SNO spectrum and other neutrino oscillation data

As mentioned previously, the SNO collaboration does not analyze the full spectrum data. We prefer, instead, to consider this information as well. We therefore consider the full SNO phase-II and phase-III data (listed in table [1]). The  $\chi_{\text{spect, SNO}}^2$  has the same formal expression as eq. 10, where it is understood that  $\mathbf{R}^{\text{th, exp}}$  are now length 26 containing two 13-bin relative to the two SNO data sets. We consider the two fully correlated.

The difficulty in using the spectrum data lies in correctly estimating the systematics. By using the information contained in table II of [8], we have computed the influence of all the different sources of error on our response function considering the correlation/anti-correlation as presented in table 1 of

[19]. The different backgrounds present yet another difficulty, because we have access only to the total number of background events coming from the different sources listed in table I of [8]. We have taken the background spectrum presented in the phase-II paper and normalized it to the total number of events in the  $D_2O + NaCl$  phase.

## 5 Our results

In table [3] we report the values of the mixing parameters  $\Delta m_{\odot}^2$ ,  $\tan^2 \theta_{\odot}$ , and the  $\chi^2$  obtained from minimization and from the peak of marginal likelihood distribution.

In fig. [1-(left)] we show the exclusion plots for the solar, radiochemical + Cherenkov solar data and KamLAND with the global signal of the SNO phase-II data, whereas the right pannel refers to the KamLAND spectrum, radiochemical + cherenkov solar data and the SNO phase-II spectrum information. Contour lines correspond to the the allowed areas at 90, 95, 99 and 99.7% CL relative to the absolute minimum.

In fig. [2] we plot the marginalized likelihood distributions for each of the oscillation parameters  $\Delta m^2$ , and  $\tan^2 \theta$  corresponding to the Kamland Spectrum plus solar evidence. The values for the peak positions and their widths are obtained by fitting two-sided Gaussian distributions and are given in table [3.a].

## 6 Summary and Conclusions

We have presented an up-to-date analysis including the recent kamland results, the SNO-phase II spectrum and all other solar neutrino data. The (predominantly) active neutrino oscillations hypothesis has been confirmed, and the decoupling of the atmospheric  $\Delta m^2$ -solar  $\Delta m^2$  justifies a 2-flavour analysis.

Due to the increased statistics, the inclusion of the new KamLAND data determines with good accuracy the value of  $\Delta m_{\odot}^2$ , clearly selecting the LMAI solution, and brings us to a new era of precision measurements in the solar neutrino parameter space [21].

It is interesting to note that the KamLAND data alone predicts, for both their analyses, a value of  $\tan^2 \theta$  smaller than the one obtained with the previous data, and significantly different from 1, consequently making the aesthetically pleasing bi-maximal-mixing models strongly disfavored. This result confirms what was already evident in the solar neutrino data analyses. Nevertheless, improvement on the determination of  $\tan^2 \theta$  is necessary and it is known that KamLAND is only slightly sensitive to this mixing parameter. The (lower) accuracy with which we determine the solar mixing angle is evident in the marginalized likelihood plots of fig. [2]. Planning of future super-beam experiments aimed at determining the  $\theta_{13}$  and eventual CP violating phases relies on the most accurate estimation of all the mixing parameters [22]. It is expected that future solar neutrino experiments, notably phase-II SNO (higher statistics, due to be made public soon) and eventually future low energy experiments, and phase-III SNO (with helium) will further restrict the allowed range of parameters.

The use of the SNO phase-II spectrum in the data set has mainly two effects: 1) a slight reduction in the overall area of the exclusion plot and 2) a slight decrease in the best-fit  $\Delta m_{\odot}^2$ .

The decrease in the best-fit mass squared difference can be understood by the fact that by including the SNO spectrum, we increase the statistical relevance of solar neutrino data, which *prefer smaller*  $\delta m^2$ . Furthermore, the oscillation pattern (whose information is contained in the spectrum) is more sensitive to  $\Delta m^2$ .

## Acknowledgments

We would like to thank F. Terranova and M. Smy for usefull discussions. P.A and V.A. thank the

brasserie/patisserie in Rue Jean de Beauvais for providing a suitable working environment in Paris. The computations were done at the computer farm of the Università degli Studi di Milano, Italy.

## References

- [1] T. Araki *et al.* [KamLAND Collaboration], ArXiv:hep-ex/0406035.
- [2] A. B. Balantekin, V. Barger, D. Marfatia, S. Pakvasa and H. Yuksel, arXiv:hep-ph/0405019. L. Oberauer, Mod. Phys. Lett. A **19** (2004) 337 [arXiv:hep-ph/0402162].
- [3] K. Eguchi *et al.* [KamLAND Collaboration], Phys. Rev. Lett. **90**, 021802 (2003).
- [4] A. B. Balantekin and H. Yuksel, J. Phys. G **29**, 665 (2003), P. Aliani, V. Antonelli, M. Picariello and E. Torrente-Lujan, Phys. Rev. D **69** (2004) 013005 [arXiv:hep-ph/0212212]. H. Nunokawa, W. J. Teves and R. Zukanovich Funchal, Phys. Lett. B **562**, 28 (2003) J. N. Bahcall, M. C. Gonzalez-Garcia and C. Pena-Garay, JHEP **0302**, 009 (2003) A. Bandyopadhyay, S. Choubey, R. Gandhi, S. Goswami and D. P. Roy, Phys. Lett. B **559**, 121 (2003) M. Maltoni, T. Schwetz and J. W. Valle, Phys. Rev. D **67**, 093003 (2003) G. L. Fogli, E. Lisi, A. Marrone, D. Montanino, A. Palazzo and A. M. Rotunno, Phys. Rev. D **67**, 073002 (2003) V. Barger and D. Marfatia, Phys. Lett. B **555**, 144 (2003) P. C. de Holanda and A. Y. Smirnov, JCAP **0302**, 001 (2003) A. B. Balantekin and H. Yuksel, J. Phys. G **29**, 665 (2003).
- [5] J. N. Bahcall, M. H. Pinsonneault and S. Basu, Astrophys. J. **555**, 990 (2001).
- [6] P. Aliani, V. Antonelli, M. Picariello and E. Torrente-Lujan, Phys. Rev. D **69** (2004) 013005 [arXiv:hep-ph/0212212.] P. Aliani, V. Antonelli, M. Picariello and E. Torrente-Lujan, New J. Phys. **5**, 2 (2003). P. Aliani, V. Antonelli, R. Ferrari, M. Picariello and E. Torrente-Lujan, Phys. Rev. D **67**, 013006 (2003). P. Aliani, V. Antonelli, M. Picariello and E. Torrente-Lujan, Nucl. Phys. B **634**, 393 (2002).
- [7] M. B. Smy, arXiv:hep-ex/0202020.
- [8] S. N. Ahmed *et al.* [SNO Collaboration], Phys. Rev. Lett. **92** (2004) 181301 [arXiv:nucl-ex/0309004].
- [9] A. W. Poon [SNO Collaboration], arXiv:nucl-ex/0110005.
- [10] Q. R. Ahmad *et al.* [SNO Collaboration], Phys. Rev. Lett. **89** (2002) 011301, Q. R. Ahmad *et al.* [SNO Collaboration], Phys. Rev. Lett. **89** (2002) 011302.
- [11] R. Davis, Prog. Part. Nucl. Phys. **32** (1994) 13. B.T. Cleveland *et al.*, (HOMESTAKE Coll.) Nucl. Phys. (Proc. Suppl.) **B 38** (1995) 47. B.T. Cleveland *et al.*, (HOMESTAKE Coll.) Astrophys. J. **496** (1998) 505-526.
- [12] J.N. Abdurashitov *et al.* (SAGE Coll.) Phys. Rev. Lett. **83**(23) (1999)4686.
- [13] A.I. Abazov *et al.* (SAGE Coll.), Phys. Rev. Lett. **67** (1991) 3332. D.N. Abdurashitov *et al.* (SAGE Coll.), Phys. Rev. Lett. **77** (1996) 4708. J.N. Abdurashitov *et al.*, (SAGE Coll.), Phys. Rev. **C60** (1999) 055801; astro-ph/9907131. J.N. Abdurashitov *et al.*, (SAGE Coll.), Phys. Rev. Lett. **83** (1999) 4686; astro-ph/9907113.
- [14] P. Anselmann *et al.*, GALLEX Coll., Phys. Lett. **B 285** (1992) 376. W. Hampel *et al.*, GALLEX Coll., Phys. Lett. **B 388** (1996) 384. T.A. Kirsten, Prog. Part. Nucl. Phys. **40** (1998) 85-99. W. Hampel *et al.*, (GALLEX Coll.) Phys. Lett. **B 447** (1999) 127. M. Cribier, Nucl. Phys. (Proc. Suppl.) **B 70** (1999) 284. W. Hampel *et al.*, (GALLEX Coll.) Phys. Lett. **B 436** (1998) 158. W. Hampel *et al.*, (GALLEX Coll.) Phys. Lett. **B 447** (1999) 127. see also new data in <http://neutrino2004.in2p3.fr/>
- [15] M. Altmann *et al.* (GNO Coll.) Phys. Lett. **B490** (2000) 16-26.

- [16] J. Boger *et al.* [SNO Collaboration], Nucl. Instrum. Meth. A **449**, 172 (2000)
- [17] G.L. Fogli, E. Lisi, A. Palazzo, A.M. Rotunno, Phys. Rev. D **67**, 073001 (2003)
- [18] G. L. Fogli, E. Lisi, A. Marrone and A. Palazzo, Phys. Lett. B **583** (2004) 149 [arXiv:hep-ph/0309100].
- [19] “HOWTO use the SNO Salt Flux Results,” [SNO Collaboration], can be found at <http://www.sno.phy.queensu.ca>
- [20] “Multinomial Goodness-of-fit Tests.”, N. Cressie and T. Read. J. R. Statist. Soc. B, 46(3):440-464, 1984.  
“Goodness-of-Fit Statistics for Discrete Multivariate Data.”, T. Read and N. Cressie. Springer Series in Statistics. Springer Verlag, New York, 1988.
- [21] see <http://neutrino2004.in2p3.fr> for KamLAND transparencies and Global analysis (S. Goswami)
- [22] V. Antonelli, M. Picariello, F. Terranova, E. Torrente-Lujan, work in progress
- [23] M. Apollonio *et al.* (CHOOZ coll.) Phys. Lett. **B 466** (1999) 415; M. Apollonio *et al.*, Phys. Lett. **B 420** (1998) 397.
- [24] Y. F. Wang [Palo Verde Collaboration], Int. J. Mod. Phys. A **16S1B**, 739 (2001); F. Boehm *et al.*, Phys. Rev. D **64**, 112001 (2001).



$T_{eff}$ (MeV)	Events per 500 keV	$T_{eff}$ (MeV)	Events per 500 keV
5.5- 6.0	510	9.0- 9.5	130
6.0- 6.5	515	9.5-10.0	120
6.5- 7.0	475	10.0-10.5	60
7.0- 7.5	385	10.5-11.0	70
7.5- 8.0	300	11.0-11.5	40
8.0- 8.5	240	11.5-12.0	35
8.5- 9.0	145		

<sup>†</sup> It contains the CC, ES, and NC + internal and external source neutron events.

Table 1: Energy spectrum observed at SNO (taken from fig. 2 of ref [8]).<sup>†</sup>

<b>Experiment</b>	<b>References</b>
Homestake	[11]
SAGE	[12, 13]
GallEx	[14]
GNO	[15]
SuperKamiokande	[7]
SNO	[8–10]
CHOOZ	[23]
Palo Verde	[24]
KamLAND	[1, 3]

Table 2: References from where we draw the data used in our analysis

	$\Delta m^2(\text{eV}^2)$	$\tan^2 \theta$
from $\chi^2$ minimization		
KL (Sp+Gl)+Solar + SNO (Sp)	$7.89 \times 10^{-5}$	0.40
KL (Sp+Gl)+Solar + SNO (Gl)	$8.17 \times 10^{-5}$	0.40
from marginalization		
KL (Sp+Gl)+Solar + SNO (Sp)	$8.2_{-0.8}^{+0.9} \times 10^{-5}$	$0.50_{-0.6}^{+0.12}$

Table 3: Mixing parameters from  $\chi^2$  minimization and likelihood marginalization.

Bin (MeV)	$S_{\text{exp}}/\text{MC}$	$\sigma_{\text{stat.}} (\%)$
2.600 - 3.025	0.45	1.4
3.025 - 3.450	0.56	1.5
3.450 - 3.875	0.67	1.7
3.875 - 4.300	0.62	2.1
4.300 - 4.725	0.99	2.6
4.725 - 5.150	1.20	3.3
5.150 - 5.575	0.80	4.5
5.575 - 6.000	1.00	6.7
6.000 - 6.425	1.20	10.0
6.425 - 6.850	0.33	17.0
6.850 - 7.275	0.67	33.0
7.275 - 7.700	0.00	-
7.700 - 8.125	-	-

Table 4: Summary of Kamland spectrum information extracted from [1]. Relative statistical errors only are reported.

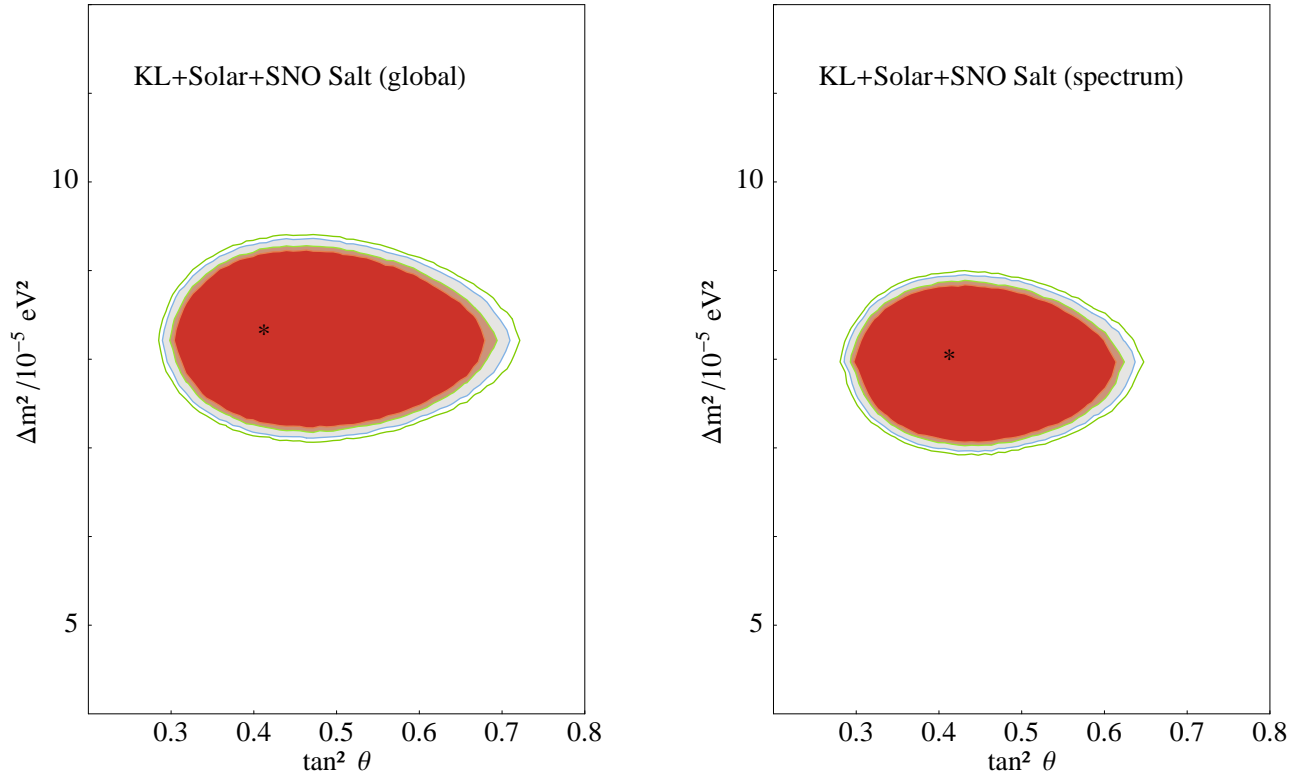


Figure 1: (*left*) Allowed region in the  $(\tan^2 \theta, \Delta m_{\odot}^2)$  plane for the global analysis, which includes the previous solar data (see e.g. [6] for details) and all KamLAND Global results. (*right*) Best fit solution for the spectrum analysis, including all previous solar data, short baseline reactor data and the KamLAND spectrum. Best fit point given in table [3].

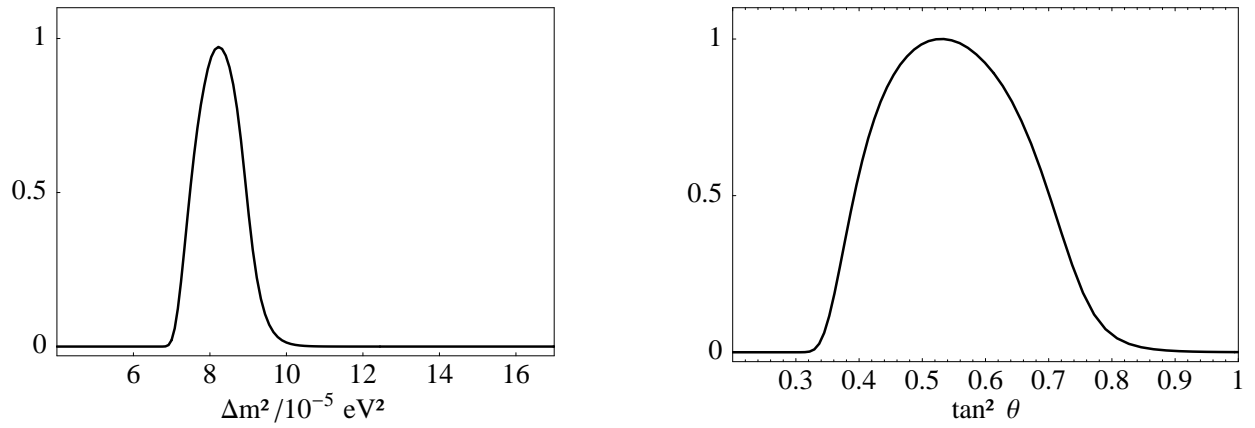


Figure 2: marginalized likelihood distributions for each of the oscillation parameters  $\Delta m^2_{\odot}$  (left) and  $\tan^2 \theta$  (right) corresponding to the totality of solar and KamLAND data. The curves are in arbitrary units with normalization to the maximum height.